Corresponding author , Anissa Célina Bouali

Highlights

- Sol-gel post-treatment was performed on a plasma electrolytic oxidation coating
- Successful growth of layered double hydroxides on plasma electrolytic oxidation post-treated by sol-gel method
- Intercalation of the obtained layered double hydroxide film with a model corrosion inhibitor “vanadate”
- Improvement of the overall corrosion resistance of the coating

Graphical abstract

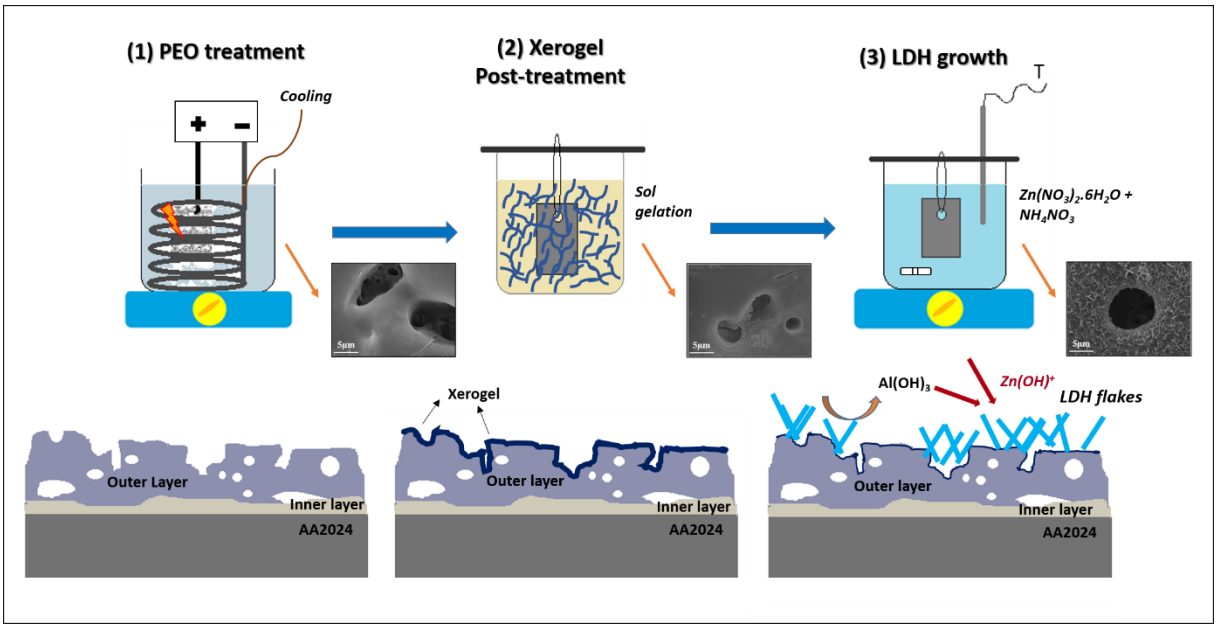

Layered double hydroxide based active corrosion protective sealing of plasma electrolytic oxidation/sol-gel composite coating on AA2024

A.C. Bouali[*a], E.A. Straumal[b], M. Serdechnova[a], D.C.F. Wieland[a], M. Starykevich[c], C. Blawert[a], J.U. Hammel[a], S.A. Lermontov[b], M. G .S. Ferreira, M.L. Zheludkevich[a,d]

[a] Institute of Materials Research, Helmholtz-Zentrum Geesthacht, Max-Planck-Straße 1, 21502 Geesthacht, Germany.

[b] Institute of Physiologically Active Compounds, Russian Academy of Sciences, 1 Severnii pr., 142432 Chernogolovka, Russia.

[c] Department of Materials and Ceramic Engineering, CICECO - Aveiro Institute of Materials, University of Aveiro, 3810-193 Aveiro, Portugal.

[d] Faculty of Engineering, Kiel University, Kaiserstraße 2, Kiel 24143, Germany.

Abstract

This work reports a novel approach for growing layered double hydroxide (LDH) films on any plasma electrolytic oxidation (PEO) coated AA2024 independently of the nature of the PEO coating. The specific PEO coating chosen to carry out this work is considered to be not suitable for direct LDH growth because of phase composition and morphological features. In this paper, we describe a new methodology that consists of covering the PEO coating with a thin layer of aluminum oxide based xerogel as the source of aluminate ions for subsequent *in-situ* LDH growth. X-ray diffraction (XRD) and scanning electron microscope (SEM) images showed a successful formation of LDHs on the surface. An improvement in terms of active corrosion protection was also demonstrated by electrochemical impedance spectroscopy (EIS) and scanning vibrating electrode technique (SVET).

Keywords: Plasma electrolytic oxidation, xerogel, layered double hydroxide, corrosion protection

[*] Corresponding author: Tel. /Fax: +49 4152 87-1943/ 1960 email: anissa.bouali@hzg.de

1. Introduction

Plasma electrolytic oxidation is a green anodizing process using micro-discharges to produce hard and dense ceramic-like coatings with a good wear and corrosion resistance [1-3]. However, the discharges are also responsible for creating defects and pores that can lead to a decrease of the barrier properties provided by the coatings and their failure in long-term corrosion protection. Different methods such as optimization of the process parameters (variation of voltage/current magnitude, mode, frequency and duty cycle) [4-6] on one hand and the addition of various particles into the electrolyte on the other hand, have been investigated to overcome the problem [8]. Yet, this optimization do not entirely prevent the presence of the porosity, besides it could significantly affect the PEO process (voltage breakdown, discharge intensity and density) which in turn can influence the final microstructure of the PEO coating [7-8].

Several approaches based on non-toxic post-treatments to seal the pores of PEO coated Mg and Al alloys were developed. Among these approaches is the conventional hydrothermal treatment, where anodized substrates are immersed in hot (96°C -100°C) deionized water to induce the formation of a hydrated oxide and close the pores [9-10]. Narayanan et *al*. relied on a similar process but improved the post-treatment by decreasing the temperature to 60°C and using an alkaline solution. The process helped to seal the smaller pores, to reduce the size of the bigger sized pores, and to provide a better homogeneity to the coating [11]. Along with these methods, sealing by means of an organic top-coat such as epoxy resins and hybrid sol-gel layers has been also disclosed in a number of works [12-16]. Although the described methods can seal the pores efficiently, they fail to maintain a long-term anti-corrosion performance when subjected to damages or degradation and become permeable to corrosive species.

In this respect, other authors resorted to the use of active anti-corrosion agents to reinforce the corrosion protection of PEO coatings. Sun et *al*. have recently discussed the utilization of cerium nitrate and benzotriazole in an immersion post-treatment of PEO coated commercially pure Mg. The results revealed an enhanced corrosion protection owed to the sealing of the pores by $Ce(NO_3)_3$ whereas the benzotriazole has not shown any positive outcome [17]. Post-treatment relying on the use of rare earth metals such as cerium [18-19] for sealing purposes have been previously tested and proven to be effective. However, the method remains unsustainable since in most cases the corrosion inhibitors absorbed into the pores can be

easily detached or react with the environment even in absence of corrosion activity, hence leading to the loss of the corrosion inhibiting capacity of the PEO coating.

In this respect, a growing interest has been accorded to smart delivery systems that can act as reservoirs for corrosion inhibitors and release them when triggered by relevant changes in the environment such as the presence of corrosive species, changes in pH or even mechanical damage. Layered double hydroxide (LDH) are promising nanocontainers that belong to the class of anionic-exchangers which structure is that of brucite $Mg(OH)_2$. Part of the divalent metal cations are replaced by trivalent ions giving positively charged layers that are balanced by the intercalation of anions in the hydrated interlamellar region [20]. Their aptitude to be loaded with corrosion inhibitors and promote effective active corrosion protection for bare [21-23] and anodized/PEO coated metals [24-27] have been intensively exploited especially for aluminum alloys.

Nonetheless, it was found that in the case of PEO coated aluminum alloys the direct LDH growth is highly contingent on the nature of the PEO coating. Two important criteria were reported to determine the LDH growth on PEO coated AA2024: i) the γ-Al_2O_3 and α-Al_2O_3 crystalline phases of the PEO coating cannot be dissolved, hence used as source for LDH formation [28] and ii) the LDH growth depends on the tortuosity of the PEO coating and the accessibility of $Al(OH)_4^-$ anions through the PEO pores. For instance, a thicker and more compact PEO coating obtained at higher voltages (~ 400-500V) has proven to be challenging or even unsuitable for LDH formation [28].

In this paper, a solution to enable the growth of LDH independently on the nature and thickness of the PEO coating is presented. An additional sol-gel based post-processing was applied in order to create an aluminum oxide based xerogel layer [29-30] offering a new source of $Al(OH)_4^-$ anions for the formation of LDH nanocontainers.

In this respect, the concept of combining high barrier properties of a thicker PEO coating and active corrosion protection provided by the LDH loaded with corrosion inhibitors (vanadate was used in frame of this work as a model corrosion inhibitor) should be achieved.

2. Material and methods

2.1.Chemicals.

The materials used in frame of this work are listed as following: aluminum nitrate nonahydrate ($Al(NO_3)_3 \cdot 9H_2O$, >99%, Sigma-Aldrich, Germany), propylene oxide (C_3H_6O, 99.5%, Sigma-Aldrich, Germany), isopropyl alcohol ($(CH_3)_2CHOH$, 99.5 %, Sigma- Aldrich,

Germany), tert-butyl methyl ether ($(CH_3)_3COCH_3$, 99%, Sigma-Aldrich, Germany), zinc nitrate hexahydrate ($Zn(NO_3)_2 \cdot 6H_2O$, >99%, CarlRoth, Germany), ammonium nitrate (NH_4NO_3, >98.5%, Bernd Kraft, Germany), ammonia solution ($NH_3 \cdot H_2O$, 25%, Merck KGaA, Germany), sodium vanadate oxide ($NaVO_3$, 96%, AlfaAesar, Germany), sodium metasilicate (Na_2SiO_3, 44-47% SiO_2, Sigma-Aldrich Chemie GmbH, Germany), potassium hydroxide (KOH, >85%, Th. Geyer, Germany) and sodium phosphate tribasic (Na_3PO_4, ≥ 96%, ACROS Organics, Germany) were used as they were received without any further purification.

2.2.Substrate composition.

The nominal composition of used AA2024 samples are given (wt. %) in the table below.

Component	Al	Cu	Fe	Cr	Mg	Mn	Si	Ti	Zn	Others
Wt. %	90.7-94.7	3.8-4.9	0.5	0.1	1.2-1.8	0.3-0.9	0.5	0.15	0.25	0.15

Table 1. Nominal composition of AA2024 in wt%.

The AA2024 coupons (30mm x 20 mm x 2.5 mm) were grinded with SiC 1200 abrasive paper and rinsed with deionized water prior to PEO treatment.

2.3.Sample preparation

2.3.1. PEO treatment

The PEO process was carried out in an electrolyte composed of 3g/l KOH, 20g/l Na_2SiO_3 and 20g/l Na_3PO_4. A pulsed DC power supply in constant voltage mode was used. In this case a voltage of 450V was applied for 10min with a pulse ratio of t_{on}/t_{off}=1ms/9ms at maximum current of 0.5A. The electrolyte was constantly stirred and maintained at 20±2 °C by a water cooling system.

2.3.2. Sol-gel post-treatment (PEO-X)

The obtained PEO samples were immersed in aluminum oxide sols that were prepared according to [29]. Briefly, 0.0123 mol of $Al(NO_3)_3 \cdot 9H_2O$ was dissolved in 20 ml of isopropanol and then 0.135 mol of propylene oxide was added. The mixture was stirred for 2 min before immersing the PEO samples for 24h at room temperature. Finally, the samples were removed, washed with *tert*-butyl methyl ether, and then dried under ambient conditions.

2.3.3. LDH formation (PEO-X-LDH)

The PEO samples with the applied xerogel layer were subjected to hydrothermal LDH conversion method using the same procedure described in previous work [24-25, 28]. Succinctly, i) Zn-Al LDH-nitrate (PEO-X-LDH-NO_3) was grown in a solution of $Zn(NO_3)_2 \cdot 6H_2O$ (0.1 M) and NH_4NO_3 (0.6 M) (pH adjusted to 6.5 using 1% ammonia) under 95 °C for 30 min, ii) Zn-Al LDH-vanadate (PEO-X-LDH-VO_x) was obtained by anion exchange reaction in a solution of 0.1 M $NaVO_3$ at pH 8.4 (50 °C for 30 min).

Aside from the PEO samples covered with xerogel, another set of reference PEO samples without xerogel treatment underwent a direct LDH growth following the same procedure.

2.4.Material characterization.

2.4.1. Surface characterization and phase analysis

A Tescan Vega3 SB scanning electron microscope (SEM, Brno, Czech Republic) equipped with an *eumeX* energy dispersive X-ray (EDS, Heidenrod, Germany) spectrometer was used to obtain images of the specimen surface and their elemental composition. The specimens were studied in both top and cross-sections views.

In addition to the SEM-EDX, tomographic data was obtained at the imaging beamline (IBL) P05 at PETRA III storage ring (DESY, Hamburg, Germany). The indirect detector system consists of a CdWO4-scintillator converting the X-rays into visible light which is magnified by a factor of 9.9 with microscope optics mounted on a back-illuminated camera system [31-32]. For measurements, an X-ray energy of 28.5keV was used with a field of view of 3.7 x 3.7 mm. The detector used is a CMOS camera with 5120 x 3840 pixels and a linear pixel size of 6.4 µm. For tomographic reconstruction, a filtered back projection using ASTRA was employed. Surface area analysis was done with the programs ImageJ and Avizo.

The phase composition and structure was investigated using a Bruker D8 Advance diffractometer (Karlsruhe, Germany). The measurement (with a Cu K_α radiation, step size 0.02°, dwell time 1s) was carried at room temperature with an incident angle set to 3°.

The glow discharge optical emission spectroscopy (GDOES) depth profile analysis of the coatings was performed with a HORIBA GD-Profiler 2 (Longjumeau, France) using a 4 mm anode, an operating pressure of 650 Pa and a power of 30W.

2.4.2. Electrochemical and corrosion assessment

The corrosion performance of the different specimens was examined using a Gamry instrument interface 1000E potentiostat (Warminster, Pennsylvania, USA). The electrochemical impedance spectroscopy (EIS) measurements were conducted inside a

Faraday cage at room temperature using a three-electrode cell with a saturated Ag/AgCl reference electrode, a platinum wire counter electrode and the differently treated aluminum samples as working electrodes. The electrolyte was a 0.5 % NaCl aqueous solution. All the spectra were recorded at open circuit potential (OCP) in a frequency range from 100000 Hz to 0.01 Hz and with a 10 mV RMS sinusoidal perturbation using 9 measuring points per frequency decade. The impedance plots were fitted using different equivalent circuits with the Gamry Echem Analyst software.

Scanning vibrating electrode technique (SVET) measurements were carried out using Applicable Electronics Inc. (New Haven, USA) instrument controlled with ASET-LV4 software from Science Wares (Falmouth, Massachusetts, USA). The measurements were performed in a 0.05 M NaCl solution using a Pt/Ir vibrating probe with a tip that was platinized to form a sphere with an average diameter of 15 µm. The SVET probe was maintained at a distance of 100 µm form the surface and the size of the collected maps were 800 µm x 1000 µm. The final obtained data was reconstructed into maps using the free Quickgrid program.

3. Results and Discussion

3.1.Structure and morphology

SEM cross-section micrograph of the PEO coating is shown in **Fig 1.a**. The coating contains a number of pores, cracks and defects, which were developed due to discharges during the PEO process. However according to the literature and the present results, the choice of the electrolyte in terms of the composition and concentration of phosphate and silicate played a role on the final morphology. Studies reported that a higher concentration of phosphate in the electrolyte generally favors the production of a more compact and stable PEO coating but leads to the creation of more cracks and larger pores whereas silicates induces higher numbers of pores but smaller in size. A combination of phosphate with silicates in equal amounts resulted in the production of a compact and thicker coating with a lower number of pores [33-35], see **Fig. 1.a**. The XRD pattern (**Fig. 1.b**) shows a broad signal at ~15 to 35° corresponding to a potential amorphous phase and some characteristic peaks related to the aluminum substrate.

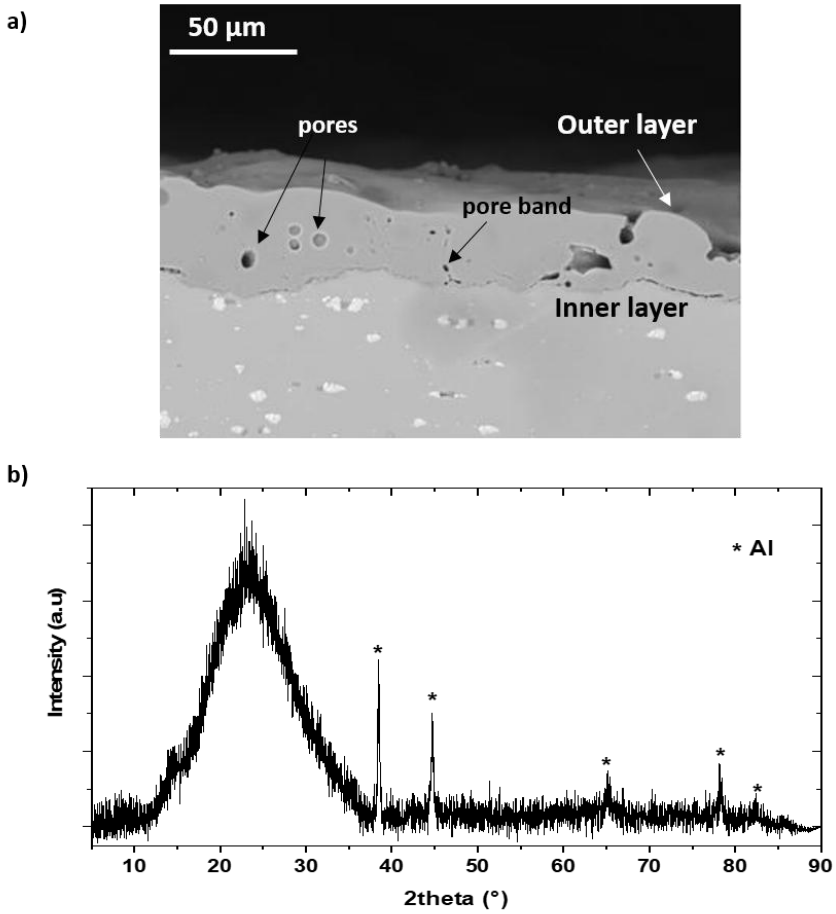

Fig. 1. SEM cross section view (a) and XRD pattern (b) of the PEO coated AA2024.

SRµCT experiments were performed to estimate the ratio between the surface area of the compact sample (bare) and porous PEO surface of the formed layer. Furthermore, the pore size distribution was calculated. The tomography studies (**Fig. 2**) performed on the PEO covered AA2024 allow a clear differentiation between the AA2024 alloy (light grey area with bright inclusions) and the PEO layer (dark grey region) grown on the surface. The SRµCT measurements show a thickness of 50µm of the PEO layer with irregular shaped pores. For a qualitative analysis, the data was segmented into background, PEO layer and bulk material. Afterwards the surface area of the AA2024 and the pores was determined by Avizo using the connected components and label analysis plugins. This analysis revealed a surface area of 1.33 mm^2 for the compact bare surface and area of 6.8 mm^2 for the outer porous layer and these values include the calculation from both closed and open pores. Furthermore, a broad pore size distribution of (28 ± 23) μm^3 was determined using tomography. (**Fig. 2.d**)

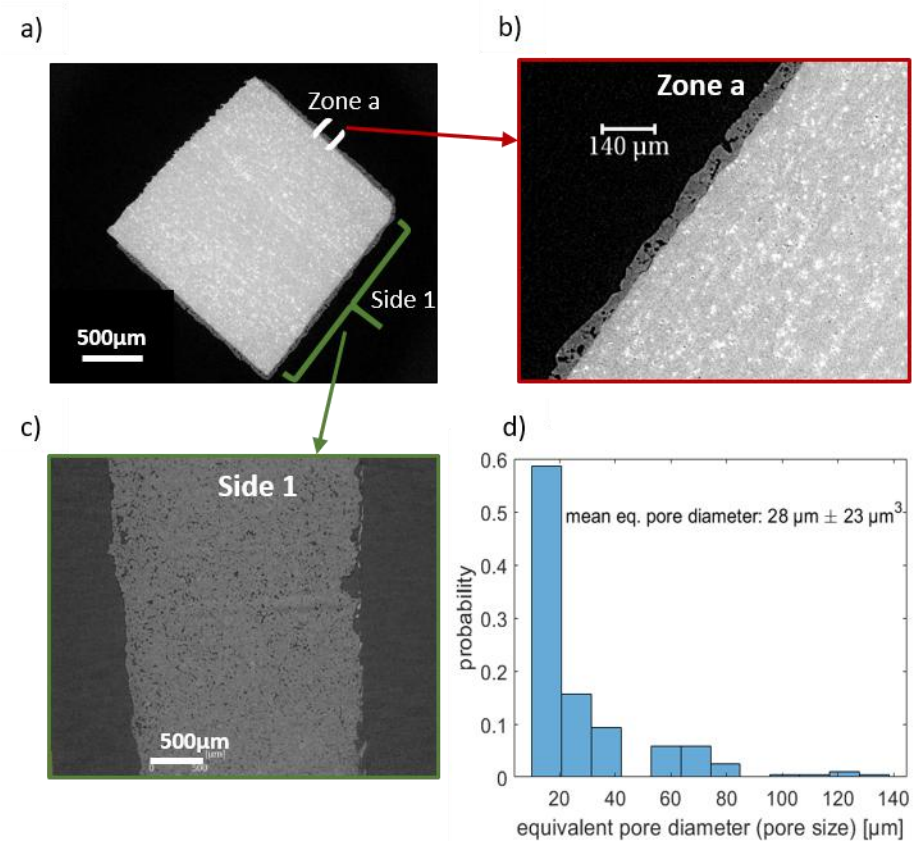

Fig. 2. Slices through the tomographic reconstructed volume showing a slice in the orthogonal direction (a) and a magnification of a small area of it– zone a (b) and along the PEO coating on one of the sides – side 1 (c) ; Histogram of the pore size distribution of the PEO coating (d)

After characterization of the PEO coated samples, an attempt to grow LDH on the latter without any prior pre-treatment was performed. The results are depicted in **Fig. 3**.

Fig. 3.a and **b** show the SEM micrographs of the PEO coated AA2024 before and after an attempt to grow LDH-NO_3 on the surface. The planar view SEM images of the PEO coated sample (**Fig. 3.a)** support the previous statement regarding the porosity and nature of the obtained PEO coating. Pores which developed due to the discharges or sparking during the treatment can be observed on the surface of the PEO-treated aluminum alloy. Following the LDH treatment no changes on the PEO surface are noticed (**Fig. 3.b)**

The additional XRD measurements (**Fig. 3.c)** did not reveal any distinctive peaks coming from LDH, and this together with SEM images support the hypothesis that the characteristics of the chosen PEO coating in terms of tortuosity and thickness is indeed not suitable for LDH formation.

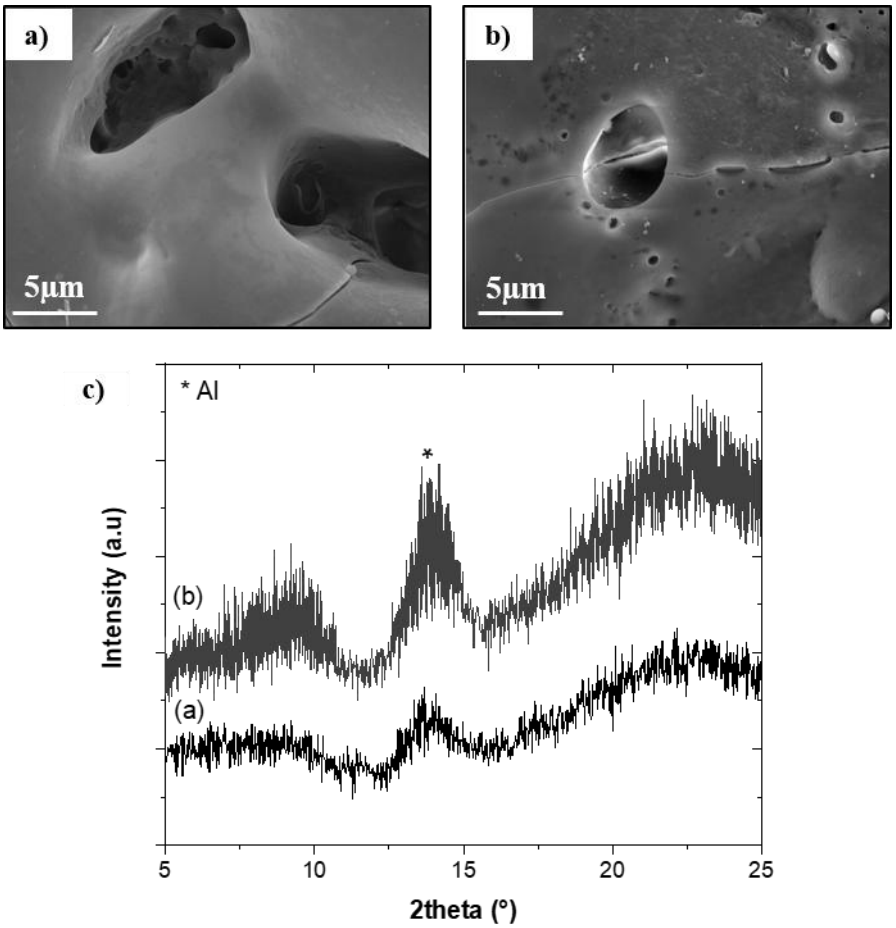

Fig. 3. SEM micrographs of PEO sample before (a) and after treatment with LDH-NO_3 (b) followed by the X- ray diffraction patterns of the PEO sample before and after treatment with LDH-NO_3 represented by the letters "a" and "b" on the figure, respectively (c)

After demonstrating the unfeasibility of LDH growth on this PEO coated AA2024, an intermediate step prior to the LDH growth consisting of a sol-gel treatment, was introduced.

Fig. 4.a represents the PEO sample after formation of a xerogel layer. Compared to the PEO micrographs without xerogel (see **Fig. 3.a**), a deposition of a fine layer in form of an assembly of small particles can be distinguished on the SEM images notably around the pores.

The thickness of the xerogel layer was estimated by the weight difference method. In other words, the samples were weighted before and after sol-gel treatment, an average value of 0.6 mg was obtained. Knowing the dimensions of the samples and the density of the obtained xerogel layer (1.23 g/cm^2), this will lead to a thickness of the xerogel layer of approx. equal to 330 nm. In this calculations, the porosity and roughness of the PEO coating were not considered, which is why we are talking about maximum possible thickness of xerogel layer if the latter would be continuously distributed. In reality (based on the SEM results presented in **Fig. 4**) one can see that there are zones with thicker agglomerations of xerogel (mostly around

the pores). This will result in a lower thickness of the xerogel layer in some zones and difficulties to detect it with SEM.

After the LDH treatment, small flake-like structures appear and are on average homogeneously distributed on the PEO-X sample surface. It can be observed that the LDH grows all along the pores (**Fig.4.b**). The surface appearance remains the same after the LDH ion exchange with vanadate (**Fig. 4.c**).

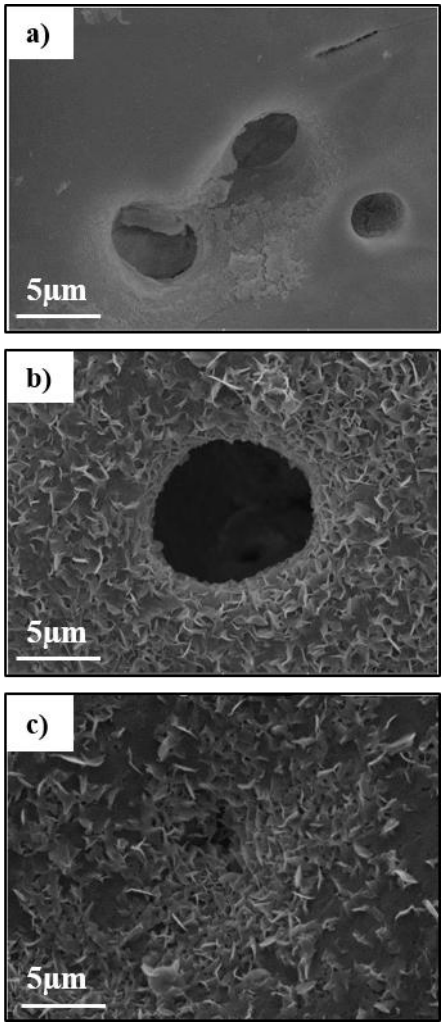

Fig. 4. SEM micrographs of PEO sample with xerogel (a) converted to LDH-NO_3 (b) and to LDH-VO_x (c).

Simultaneously after the SEM images (**Fig. 3** and **4**), EDS elemental distribution data were collected (**Fig. 5**), for the four samples of interest; PEO, PEO-X, PEO-X-LDH-NO_3 and PEO-X-LDH-VO_x.

Al (from the substrate, PEO, xerogel and LDH), P and Si from the PEO coating are present in all specimens. No difference in the elemental distribution between the PEO sample with and

without xerogel can be observed with EDS analysis since the additional xerogel layers is mostly composed of Al oxide. Zn was revealed on both PEO-X-LDH-NO_3 (**Fig. 5.c**) and PEO-X-LDH-VO_x (**Fig. 5.d**) specimens and located in regions with pores and defects of PEO coating. The same fact was described in a previous work [24]. However, in this case, it can be justified by the xerogel settling preferentially in these defected zones during the post-treatment, which consequently is followed by the LDH formation in the same zones. Vanadium was found only on the PEO-X-LDH-VO_x (**Fig. 5.d**) specimens, and is overlapping with regions where Zn is present.

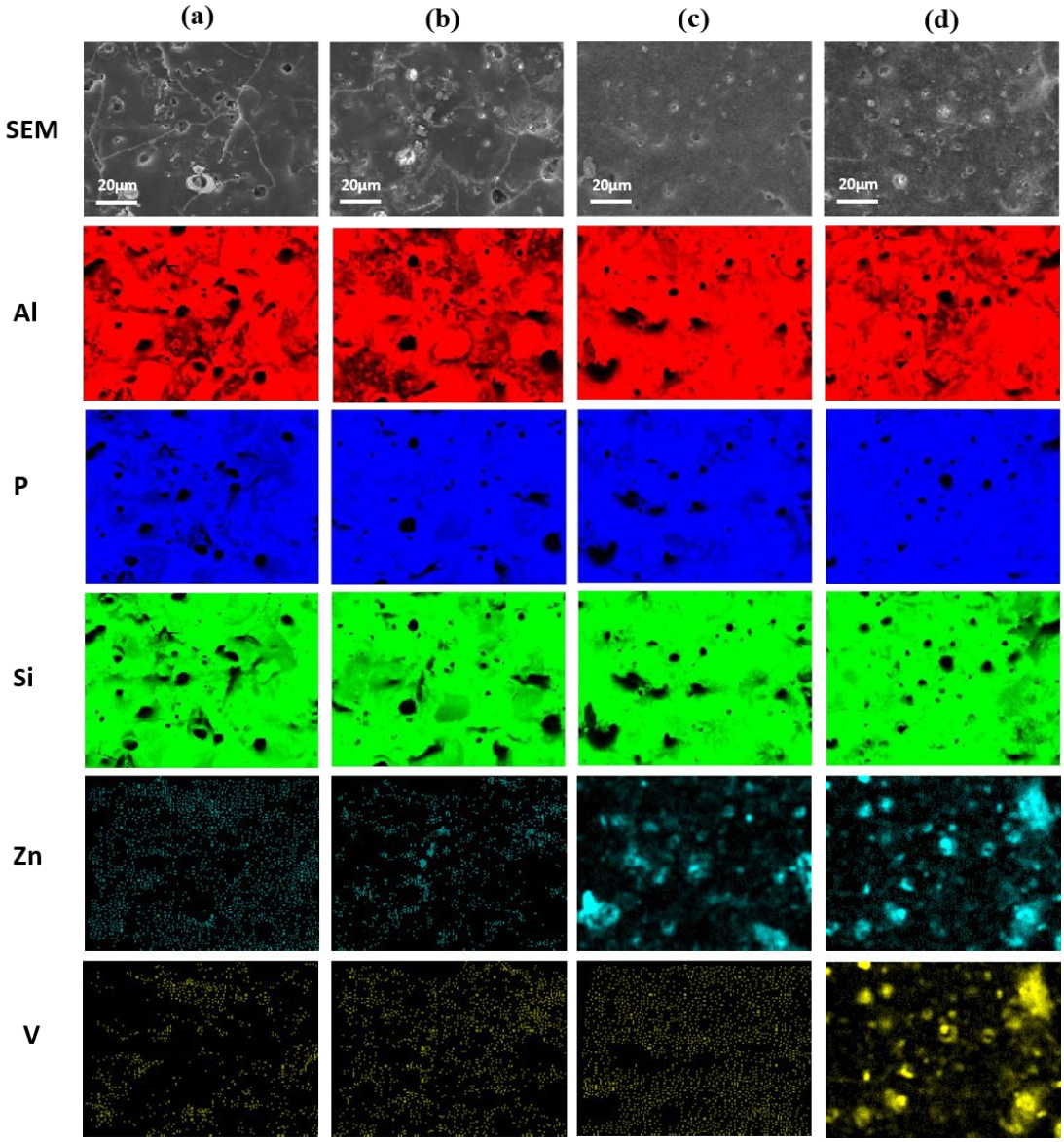

Fig. 5. EDS elemental distribution for PEO sample (a), PEO-X (b) plus PEO-X-LDH-NO_3 (c) and PEO-X-LDH-VO_x (d).

To corroborate the above results, XRD patterns of PEO sample and the as-prepared LDH films grown on PEO treated with xerogel samples were recorded and shown in **Fig. 6**. Two main distinctive reflections, (003) and (006) can be identified at 9.8° and 19.8° for the PEO-X-LDH-NO_3, entailing the formation of LDH intercalated with NO_3^-. Following anion exchange with vanadate, these reflections shift toward lower angles, 9.1° for (003) and 18.6° for (006). The reason is related to an increase of the basal spacing since the vanadate molecules are bigger then the nitrates ones. This confirms that the inhibitor anions were successfully intercalated within the LDH interlayer galleries as a result of ion exchange.

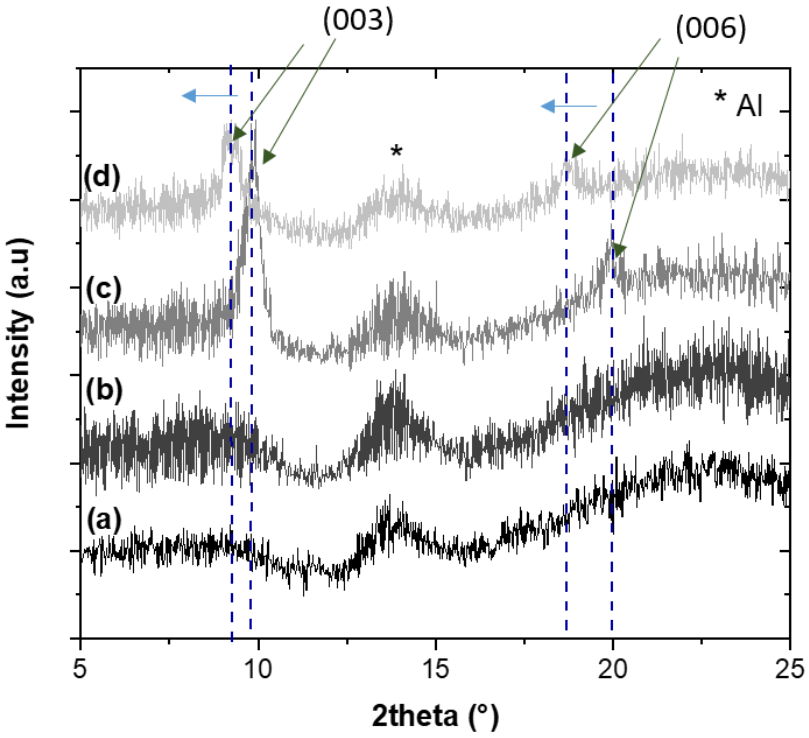

Fig. 6. X- ray diffraction patterns of PEO sample (a) PEO with xerogel (b) plus LDH-NO_3 (c) and LDH-VO_x (d).

The results of GDOES depth profile analysis are displayed in **Fig. 7**. The depth profiles show that all four samples present some difference in regards to the thickness of the film. Nonetheless, these dissimilarities are less pronounced when comparing the PEO-X-LDH-NO_3 sample to PEO-X-LDH-VO_x. The PEO sample with xerogel requires a longer plasma etching time to attain the substrate surface due to the formation of the additional xerogel layer. However, after LDH growth the thickness of the coating decreases, and this can be explained by a total or partial depletion of the xerogel layer as it is consumed for the formation of LDH nanocontainers.

The depth profile of the zinc element exhibits a flat line for the PEO and PEO-X samples through all the plasma etching duration. The signal intensity is at the background level, whereas for both PEO-X-LDH-NO_3 and PEO-X-LDH-VO_x, the values are higher at beginning and decrease when reaching the Al substrate. This confirms an increase of Zn owing to the formation of Zn-Al LDH. Furthermore, the zinc profile exhibits a small bump that can be related to a possible intersection with a pore band close to the interface and/or the presence of zinc in the pores of the PEO coating. The latter could also mean that the xerogel was introduced into the pores and then dissolved to be used for the LDH formation. It is important to mention that a direct quantitative comparison of GDOES results for different systems is not straightforward. Therefore, only qualitative trends of the element distribution through the coating depth are discussed.

The signal of vanadate can be observed only for PEO-X-LDH-VO_x compared to a vanadate signal close to background level for both PEO and PEO-X-LDH-NO_3. In this case, as well, an increase of the vanadate signal is observed at the PEO coating interface. The vanadate profile displays the same tendency as for the zinc in the presence of LDH (**Fig. 7.d**), which corroborates the assumption of the presence of LDH in the PEO pores.

In view of the gathered results, the mechanism involved in the formation of LDH films in this particular system (schematically illustrated in **Fig. 8**), can be explained gradually according to the following steps ;

a) ***Xerogel*** formation covers two different processes; the preparation of the wet gel and its

drying. There are various methods to prepare aluminum oxide wet gel [36-37]. In this work, the convenient and mild epoxide-based procedure proposed by Simpson et al. [37] was used for wet gel preparation. This procedure itself can be divided in several stages;

The first stage concerns the dissolution of the metal salt. Since, in aqueous media metal atoms M exist as solvated cations M $[H_2O]_N^{z+}$. Two types of chemical reactions occur in this solution; the hydrolysis reactions (which replace H_2O groups by OH ones with loss of protons) and condensation reactions (formation of M-O-M “oxo” bridges with elimination of water molecules). The combination of these reactions leads to formation of colloidal particles (in other words sol formation).

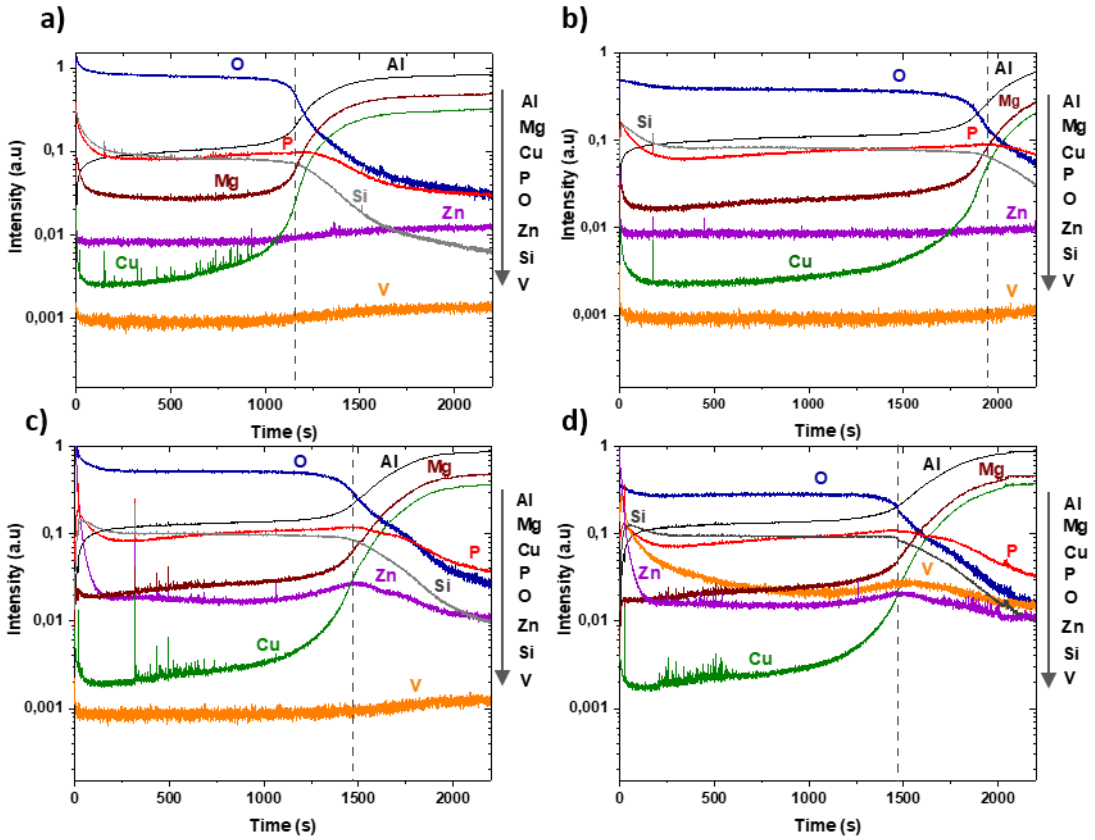

Fig. 7. GDEOS depth profiles of PEO sample (a), PEO with xerogel (b) plus LDH-NO_3 (c) and LDH-VO_x (d) separated by a dashed line to distinguish between the interface on the left side and the substrate on the right side of the profiles.

However, it should be noted that the acid formed during the hydrolysis process does not allow the reactions to proceed completely.

Al oxide gel formation occurs due to the formation of chemical bonds between sol particles (condensation process with elimination of a water molecule). Therefore, for gelation, it is necessary to promote the further condensation process.

The epoxide-assisted method is based on the ability of alkene oxides to scavenge acids irreversibly, facilitating slow and controlled aluminum salt hydrolysis and sol particles' condensation.

The above explanation are resumed in form of chemical equations (1), (2) and (3):

aluminum oxide gel formation,

$$Al\,(NO_3)_3 \cdot 9H_2O \;\rightleftharpoons\; [Al\,(H_2O)_6]^{3+} + 3NO_3^- \qquad (1)$$

$$[Al(H_2O)_6]^{3+} \rightleftharpoons\; [Al(H_2O)_6](OH)_a^{(3-a)+} \xrightarrow[-H_2O]{} Al_xO_y(OH)_z.nH_2O \qquad (2)$$

Propylene oxide scavenges protons (and counterions) and promotes further hydrolysis reaction as following,

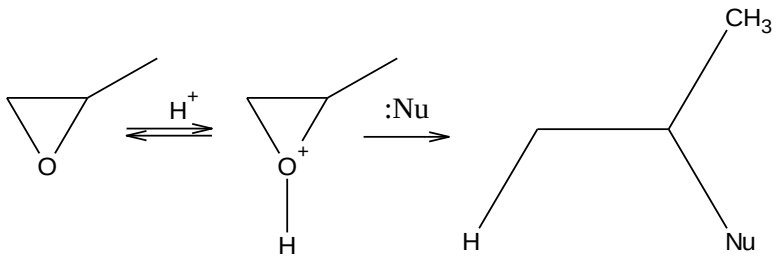

(3)

$$Nu = NO_3^-, H_2O$$

b) Subsequently to the covering of the PEO specimens with xerogel, they are immersed in a solution containing zinc and nitrate precursors for **LDH** formation [24, 25, 28].

- The LDH-NO_3 can be formed accordingly;

$$Al_xO_y(OH)_z.nH_2O + H_2O + OH^- \rightarrow xAl(OH)_4^-$$

(4)

$$Zn^{2+} + OH^- \rightarrow Zn(OH)^+$$

(5)

$$Zn(OH)^+ + xAl(OH)_4^- + NO_3^- + H_2O \rightarrow \boldsymbol{LDH - NO_3} \quad (6)$$

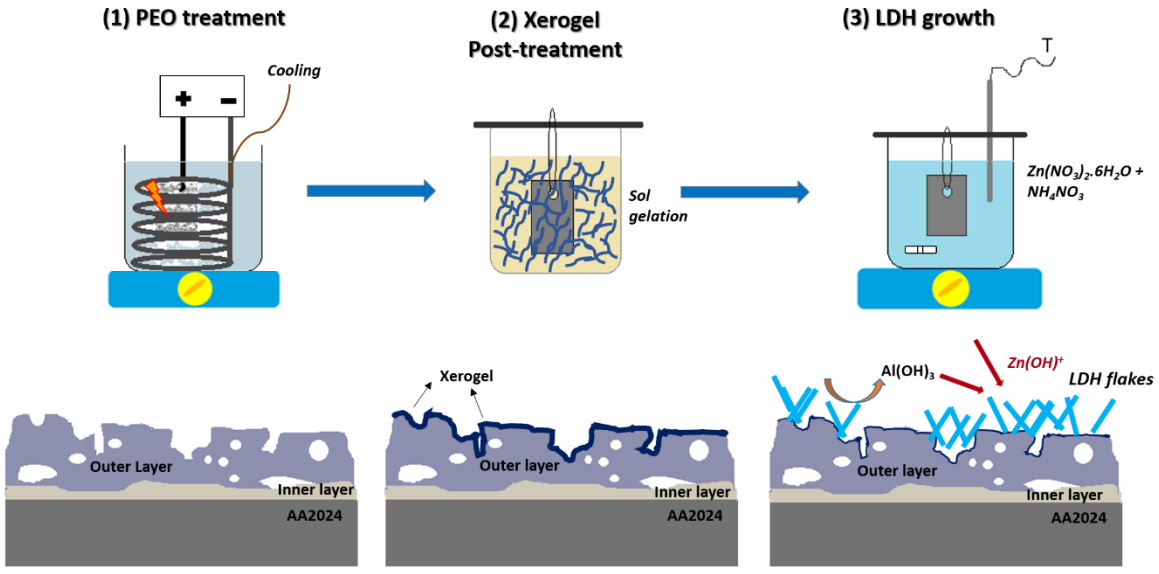

Fig 8. Scheme describing the different steps to obtain the final LDH coated PEO layer.

It is important to mention that the described mechanisms are simplistic. The actual processes taking place in the aqueous media are much more complex and are highly dependent on a number of factors namely the pH, the solution concentration, solvent, temperature, etc.

Therefore, it can be more challenging to identify the exact reaction mechanisms and that is outside the current work scope.

3.2.Electrochemical characterization

The overall corrosion resistance of the four systems was evaluated using electrochemical impedance spectroscopy (EIS). The Bode plots of the systems were recorded after 1h, 48h and 168h immersion in 0.5 % NaCl and are depicted in **Fig. 9.**

At first glance into the low frequencies (10^{-2} Hz) of the different spectra, it can be clearly seen that the impedance modulus of the different systems continuously diminishes with time. Despite that, the corrosion resistance of the PEO-X system presents a better performance than the other three systems at the beginning (1h). This can be related to the additional barrier effect offered by the xerogel layer. After 168h, the PEO-X-LDH-VO_x sample shows the highest EIS modulus.

During the first hour of immersion, the PEO coated AA2024 exhibits three time constants. The first time constant at high frequencies (Freq > 10^4 Hz) can be ascribed to a contribution of the barrier response of the outer layer and the pores that are initially not entirely filled up with solution, thus explaining the relatively high impedance at high frequencies. The second constant at mid-frequencies (10^0-10^1 Hz) represents the response from the inner barrier layer that appears to be stable during time. The time constant at lower frequencies (Freq < 10^{-1}) can be ascribed to the response from the double layer capacitance and the charge transfer resistance due to the initiated corrosion process.

The PEO-X sample shows the highest barrier protection at the start, this is probably due to the xerogel sealing properties as mentioned above. With time, the additional protection offered by the xerogel layer decreases and after 168h, it is no longer observed.

In the case of PEO-X-LDH-NO_3, no significant improvement of the impedance modulus can be noticed during the whole immersion period. Although, the LDH-NO_3 is expected to show some increase of the corrosion protection due to a sealing effect [24-25] but it is not apparent in this case. This behavior can be explained by the decrease/consumption of the xerogel layer during the synthesis of LDH, hence reducing the sealing effect that could be provided by the latter.

The PEO-X-LDH-VO_x exhibits higher impedance modulus compared to PEO and PEO-X-LDH-NO_3 samples but still lower then PEO-X at the first hour of immersion. However, after 168h it shows a better performance, while the PEO-X impedance decreases. The PEO-X-LDH-VO_x system shows fours time constant, the additional relaxation process appearing

between 10^1-10^0 Hz can be assigned to the inhibition effect of vanadate from the LDH upon release and formation of a thin protective layer [38].

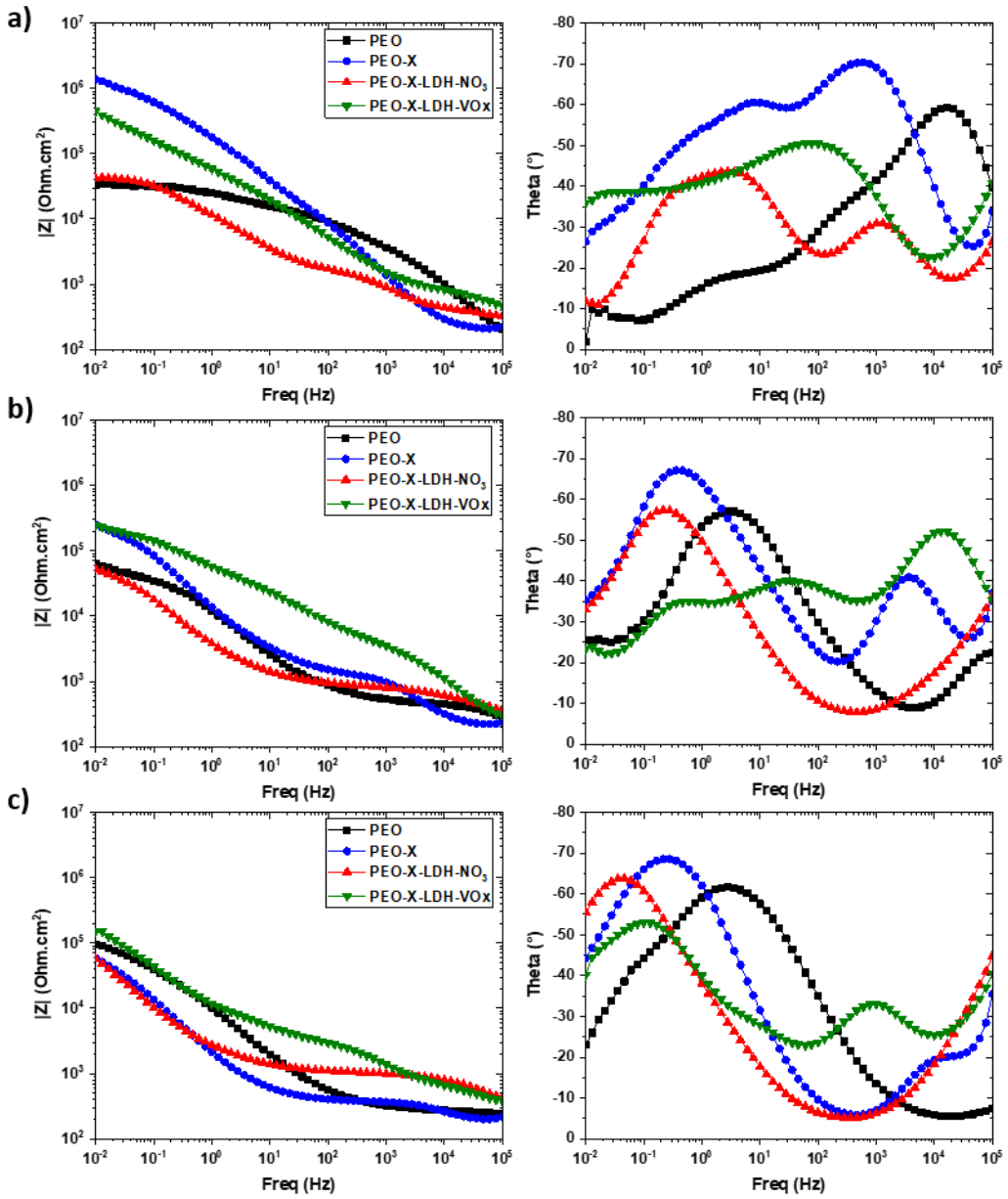

Fig. 9. Bode plots for PEO sample, PEO-X-LDH-NO_3 and PEO-X-LDH-VO_x after 1h (a), 48h (b), and 168h (c) immersion in 0.5% NaCl solution.

Localized corrosion processes was examined with the scanning vibrating electrode technique (SVET) after 4h, 12h and 22h immersion in 0.05M NaCl. In order to observe the self-healing effect on the different samples, two artificial defects of 100µm depth were drilled into the samples at a distance of 1mm from each other. The measuring probe was placed at approximately 100 µm above the sample. The SVET maps are shown in **Fig. 10**.

A clear improvement of the corrosion resistance can be noticed for the sample with LDH-VO_x. For the reference samples with only PEO, corrosion starts mainly at the defects after the first hours of immersion and spreads in other areas of the sample with time (22h). Significant corrosion activities were observed for the PEO-X samples and increase with time as it can be seen by the different cathodic and anodic regions on the map.

In the case of PEO-X-LDH-NO_3 sample and according to previous reported results [24], it was expected that the system would provide an additional protection due to the nano-trapping properties of LDH-NO_3 since it was previously disclosed that it could trap corrosive species such as Cl^- into the galleries and contribute to the reduction of corrosion reactions taking place at the interface [39-40]. Yet, this response is masked and no remarkable improvement was observed neither in the EIS nor in the SVET results. Indeed, after longer immersion times until 22h, the corrosion activity also increased for the PEO-X-LDH-NO_3 sample. Slight corrosion activity is also detected for PEO-X-LDH-VO_x in the beginning. However, it does not increase greatly after longer immersion time, which backs up the results of the preceding EIS and the idea of the functionality played by vanadate in the formation of a protective layer.

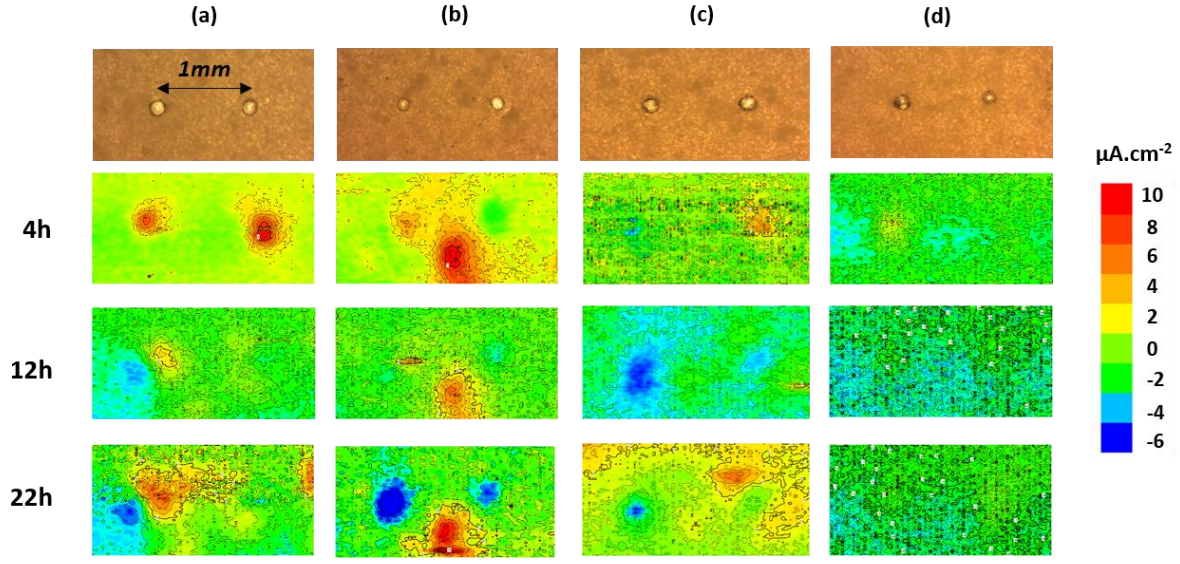

Fig. 10. Micrographs and SVET maps of PEO (a), PEO-X (b) PEO-X-LDH-NO_3 (c) and PEO-X-LDH-VO_x sample (d) after 4 h, 12 h and 22 h immersion in 0.05 M NaCl.

Considering all results, there is a clear potential for the use of xerogel as an intermediate post-treatment to enable the growth of nano-structured LDH-container layers on various range of PEO coatings, especially for the ones that are not suitable for direct LDH growth [28]. Although, we demonstrated that there is an improvement in the corrosion performance, there is still a need to develop the process further and achieve higher efficiency. This can be

achieved by first, carrying out a systematic study on PEO coatings with different morphologies to have a better grasp on how to associate an ideal barrier protection from the PEO coating itself and the sealing plus active corrosion protection from the "smart" LDH nanocontainers. Secondly, the parameters for both xerogel layer application pre-treatment on PEO and the LDH growth can be optimized (concentration, temperature, time, etc.). Moreover, one can think of other types of corrosion inhibitors with better corrosion performance and more importantly environmentally friendly which is not the case for vanadate that was used in this work as a model.

4. Conclusion

A novel approach of achieving active corrosion protection by means of LDH conversion sealing for PEO coatings has been proposed in this work. The possibility to expand the use of LDH-based sealing for different PEO coatings, regardless of their morphologies and phase composition, was demonstrated.

The approach is based on the formation of aluminum oxide consisting xerogel in the PEO pores via an intermediate sol-gel treatment step. The xerogel layer itself can act as a sealing for the PEO pores, however, it does not provide "smart" protection *on demand* as it can be done be LDH-based nanocontainers. From another hand, xerogel can be used as a source of aluminum compounds for LDH formation. In frame of this work, formed LDH nanocontainers were loaded with vanadate as a model corrosion inhibitor, in this way providing an active corrosion protection to the PEO-/LDH-based hybrid coating as it was shown during electrochemical characterization.

This work falls within the framework of future optimizations and surface functionalization to provide an active corrosion protection (and other possible functionalizations) to different materials, where LDH cannot be formed directly. Moreover, this work can be considered as a relevant step in pursuing efficient environmentally friendly corrosion protective methods especially in combination with the use of less toxic and more ecological corrosion inhibitors.

Acknowledgements

We acknowledge DESY (PETRA III, Hamburg, Germany) and GEMS (P0.5 end-station, HZG, Geesthacht, Germany) and members of the Helmholtz Association HGF, for the provision of experimental facilities for tomography measurements.

This work was partially financed by the European project MULTISURF (Marie Skłodowska-Curie, Horizon2020-RISE, grant agreement No 645676). E.A.S. and S.A.L. would like to acknowledge the financial support of the Russian Foundation for Basic Research (RFBR, grant number 18-29-06014). M.S. and C.B. would like to also thank the ACTICOAT project (Era.Net RUS Plus Call 2017, Project 477) for the financial support.

Declarations of interest: none

References

[1] A. Lugovskoy, M. Zinigrad, Plasma electrolytic oxidation of valve metals, in: Materials Science - Advanced Topics, Yizhak Mastai (Eds), InTech 201, 2013 pp. 85-102.

[2] A. Curran, T.W. Clyne, Thermo-physical properties of plasma electrolytic oxide coatings on aluminum, Surf. Coat. Technol. 199 (2005) 168–179.

[3] M. Mohedano, X. Lu, E. Matykina, C. Blawert, R. Arrabal, M.L. Zheludkevich, Plasma electrolytic oxidation (PEO) of metals and alloys, in: *Encyclopedia of Interfacial Chemistry*, 1st ed, K. Wandelt (Ed.) , Elsevier:Oxford, UK, 2018, pp. 423–438.

[4] E. Matykina, R. Arrabal, P. Skeldon, G.E. Thompson, Investigation of the growth processes of coatings formed by AC plasma electrolytic oxidation of aluminum, Surf. Coat. Technol. 54 (2009) 6767–6778.

[5] I.P. Mertsalo, V.T. Yavors'kyi, M.D. Klapkiv, R.S. Mardarevych, Wear resistance of anodic-spark coatings on aluminum alloys, Mater. Sci. 39 (2003) 136–139.

[6] V. S. Egorkin, S. V. Gnedenkov, S. L. Sinebryukhov, I. E. Vyaliy, A. S. Gnedenkov, R. G. Chizhikov, Increasing thickness and protective properties of PEO-coatings on aluminum alloy, Surf. Coat. Technol. 334 (2018) 29-42.

[7] R. Arrabal, M. Mohedano, E. Matykina, A. Pardo, B. Mingo, M. C. Merino, Characterization and wear behaviour of PEO coatings on 6082-T6 aluminium alloy with incorporated α-Al_2O_3 particles, Surf. Coat. Technol. 269 (2015) 64-73.

[8] X. Lu, M. Mohedano, C. Blawert, E. Matykina, R. Arrabal, K.U. Kainer, M. L. Zheludkevich, Plasma electrolytic oxidation coatings with particle additions – A review, Surf. Coat. Technol. 307 (2016) 1165-1182.

[9] L. Hao, B. R. Cheng, Sealing processes of anodic coatings—past, present, and future, Met Finish. 98 (2000) 8-18

[10] B. Priet, G. Odemer, C. Blanc, K. Giffard, L. Arurault, Effect of new sealing treatments on corrosion fatigue lifetime of anodized 2024 aluminium alloy, Surf. Coat. Technol. 307 (2016) 206-219.
[11] T.S. Narayanan, M.H. Lee, A simple strategy to modify the porous structure of plasma electrolytic oxidation coatings on magnesium, Rsc Adv. 6 (2016) 16100-16114.
[12] H.H. Yang, X.S. Wang, Y.M. Wang, Y. L. Wang, Z.H. Zhang, Microarc oxidation coating combined with surface pore-sealing treatment enhances corrosion fatigue performance of 7075-T7351 Al alloy in different media, Materials. 10 (2017) 609.
[13] X.S. Wang, X. W. Guo, X. D. Li, D.Y. Ge, Improvement on the fatigue performance of 2024-T4 alloy by synergistic coating technology, Materials. 7 (2014) 3533-3546.
[14] M. Zemanová, M. Chovancová, Sol-gel method for sealing anodized aluminum, Met. Finish. 101 (12) (2003) 14-16.
[15] M. Chen, S. Liu, J. Li, N. Cheng, X. Zhang, Improvement to corrosion resistance of MAO coated 2519 aluminum alloy by formation of polypropylene film on its surface, Surf. Coat. Technol. 232 (2013) 674–679.
[16] V. R. Capelossi, M. Poelman, I. Recloux, R. P. B Hernandez, H. G. De Melo, M.G. Olivier, Corrosion protection of clad 2024 aluminum alloy anodized in tartaric-sulfuric acid bath and protected with hybrid sol–gel coating, Electrochim. Acta. 124 (2014) 69-79.
[17] M. Sun, A. Matthews, A. Yerokhin, Plasma electrolytic oxidation coatings on cp-Mg with cerium nitrate and benzotriazole immersion post-treatments, Surf. Coat. Technol. 344 (2018) 330-341.
[18] F. Mansfeld, C. Chen, C. B. Breslin, D. Dull, Sealing of anodized aluminum alloys with rare Earth metal salt solutions, J. Electrochem. Soc. 145 (1998) 2792-2798.
[19] A. Carangelo, M. Curioni, A. Acquesta, T. Monetta, F. Bellucci, Cerium-Based Sealing of Anodic Films on AA2024T3: Effect of Pore Morphology on Anticorrosion Performance, J. Electrochem. Soc. 163 (2016) C907-C916.
[20] X. Duan, J. Lu, D.G. Evans, Assembly Chemistry of Anion-intercalated Layered Materials, in: *Modern Inorganic Synthetic Chemistry,* R. Xu, W. Pang, Q. Huo (Eds.), Elsevier: Amsterdam, 2011, pp. 375–404.
[21] Y. Wang, D. Zhang, Z. Lu, Hydrophobic Mg–Al layered double hydroxide film on aluminum: Fabrication and microbiologically influenced corrosion resistance properties, Colloids Surf. A. 474 (2015) 44–51.

[22] F. Zhang, C.L. Zhang, L. Song, R.C. Zeng, L.Y. Cui, H.Z. Cui, Corrosion resistance of superhydrophobic Mg–Al layered double hydroxide coatings on aluminum alloys, Acta Metall Sin-Engl. 28 (2015) 1373-1381.

[23] T. Yan, S. Xu, Q. Peng, L. Zhao, X. Zhao, X. Lei, F. Zhang, Self-healing of layered double hydroxide film by dissolution/recrystallization for corrosion protection of aluminum, J. Electrochem. Soc. 160 (2013) C480-C486.

[24] M. Serdechnova, M. Mohedano, B. Kuznetsov, C.L. Mendis, M. Starykevich, S. Karpushenkov, J. Tedim, M.G.S. Ferreira, C. Blawert, M.L. Zheludkevich, PEO coatings with active protection based on in-situ formed LDH-nanocontainers, J. Electrochem. Soc. 164 (2017) C36–C45.

[25] B. Kuznetsov, M. Serdechnova, J. Tedim, M. Starykevich, S. Kallip, M.P. Oliveira, M.L. Zheludkevich, Sealing of tartaric sulfuric (TSA) anodized AA2024 with nanostructured LDH layers, Rsc. Adv. 6 (2016) 13942-13952.

[26] F. Peng, D. Wang, Y. Tian, H. Cao, Y. Qiao, X. Liu, Sealing the Pores of PEO Coating with Mg-Al Layered Double Hydroxide: Enhanced Corrosion Resistance, Cytocompatibility and Drug Delivery Ability, Sci. Rep. 7 (2017) 8167.

[27] G. Zhang, L. Wu, A. Tang, B. Weng, A. Atrens, S. Ma, L .Liu, F. Pan, Sealing of anodized magnesium alloy AZ31 with MgAl layered double hydroxides layers, RSC Adv. 8 (2018) 2248-2259.

[28] M. Serdechnova, M. Mohedano, A.C. Bouali, D. Höche, B. Kuznetsov, S. Karpushenkov, C. Blawert, M. L. Zheludkevich, Role of Phase Composition of PEO Coatings on AA2024 for In-Situ LDH Growth, Coatings. 7 (2017) 1-7.

[29] S. A. Lermontov, E. A. Straumal, A. A. Mazilkin, I. I. Zverkova, A. E. Baranchikov, B. B. Straumal, V. K. Ivanov, How to tune the alumina aerogels structure by the variation of a supercritical solvent. Evolution of the structure during heat treatment, J. Phys. Chem. C. 120 (2016) 3319-3325.

[30] A. C. Pierre, G. M. Pajonk, Chemistry of Aerogels and Their Applications, Chem. Rev. 102 (2002) 4243-4265.

[31] A. Haibel, M. Ogurreck, F. Beckmann, T. Dose, F. Wilde, J. Herzen, M. Müller, A. Schreyer, V. Nazmov, M. Simon, A. Last, J. Mohr, Micro- and nano-tomography at the GKSS imaging beamline at PETRA III, 2010.

[32] F. Wilde, M. Ogurreck, I. Greving, J.U. Hammel, F. Beckmann, A. Hipp, L. Lottermoser, I. Khokhriakov, P. Lytaev, T. Dose, H. Burmester, M. Müller, A. Schreyer, Micro-CT at the imaging beamline P05 at PETRA III. *AIP Conference Proceedings 1741*, 1 (2016), 030035.

[33] Z.U. Rehman, S.H. Shin, M. Kaseem, M. Uzair, B.H. Koo, Towards a compact coating formed on Al6061 alloy in phosphate based electrolyte via two-step PEO process and K2ZrF6 additives, Surf. Coat. Tech. *328* (2017) 355-360.

[34] Y. Mori, A. Koshi, J. Liao, H. Asoh, S. Ono, Characteristics and corrosion resistance of plasma electrolytic oxidation coatings on AZ31B Mg alloy formed in phosphate – Silicate mixture electrolytes, Corros. Sci. 88 (2014) 254-262.

[35] L. Guohua, G. Weichao, Huan Chen, Wenran Feng, M. Latif Khosa, L. Li, Erwu Niu, Guling Zhang, Si-Ze Yang, Characteristic of ceramic coatings on aluminum by plasma electrolytic oxidation in silicate and phosphate electrolyte, Appl. Surf. Sci. 253 (2006) 2947-2952.

[36] J.F. Poco, J.H. Satcher, L.W. Hrubesh, Synthesis of high porosity, monolithic alumina aerogels, J. Non-Cryst Solids, 285 (2001) 57-63.

[37] A.E. Gash, T.M. Tillotson, J.H. Satcher, L.W. Hrubesh, R.L. Simpson, New sol-gel Synthetic Route to Transition and Main-Group Metal Oxide Aerogels Using Inorganic Salt Precursors, J. Non-Cryst. Solids. 285 (2001), 22−28.

[38] D. Mata, M. Serdechnova, M. Mohedano, C. L. Mendis, S. V. Lamaka, J. Tedim, T. Hack, S. Nixon , M. L. Zheludkevich, Hierarchically organized Li–Al-LDH nano-flakes: a low-temperature approach to seal porous anodic oxide on aluminum alloys, RSC Adv. (2017) 35357–35367.

[39] J. Tedim, A.I. Kuznetsova, A.N. Salak, M. Montemor, D. Snihirova, M. Pilz, M.L. Zheludkevich, M.G.S. Ferreira, Zn-Al layered double hydroxides as chloride nanotraps in active protective coatings. Corros. Sci. 55 (2012). 1-4.

[40] J. Tedim, A.C. Bastos, S. Kallip, M.L. Zheludkevich, M.G.S. Ferreira, Corrosion protection of AA2024-T3 by LDH conversion films. Analysis of SVET results, Electrochim. Acta . 210 (2016) 215-224.

Graphical Abstract

Click here to download high resolution image

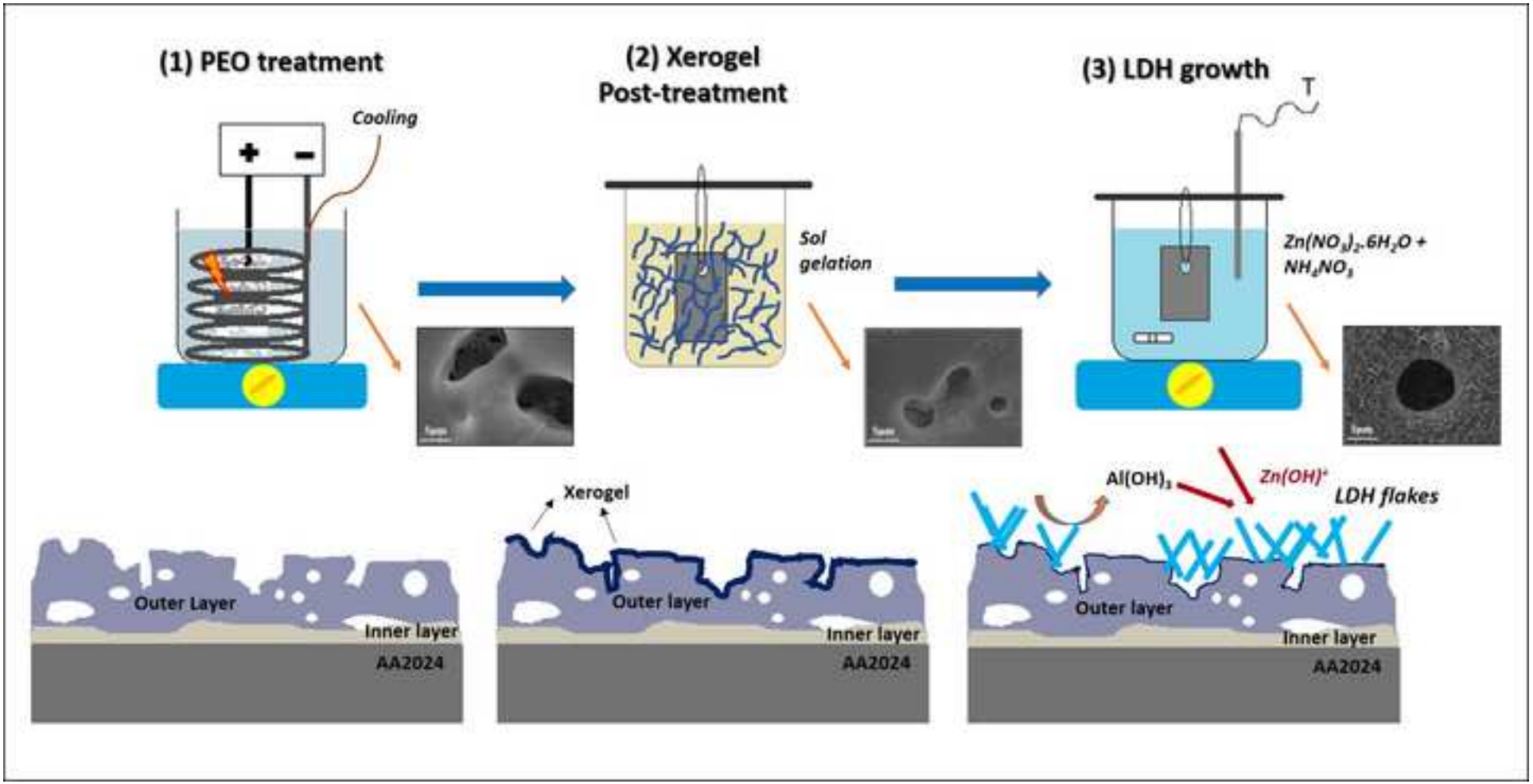

Figure 1

Click here to download high resolution image

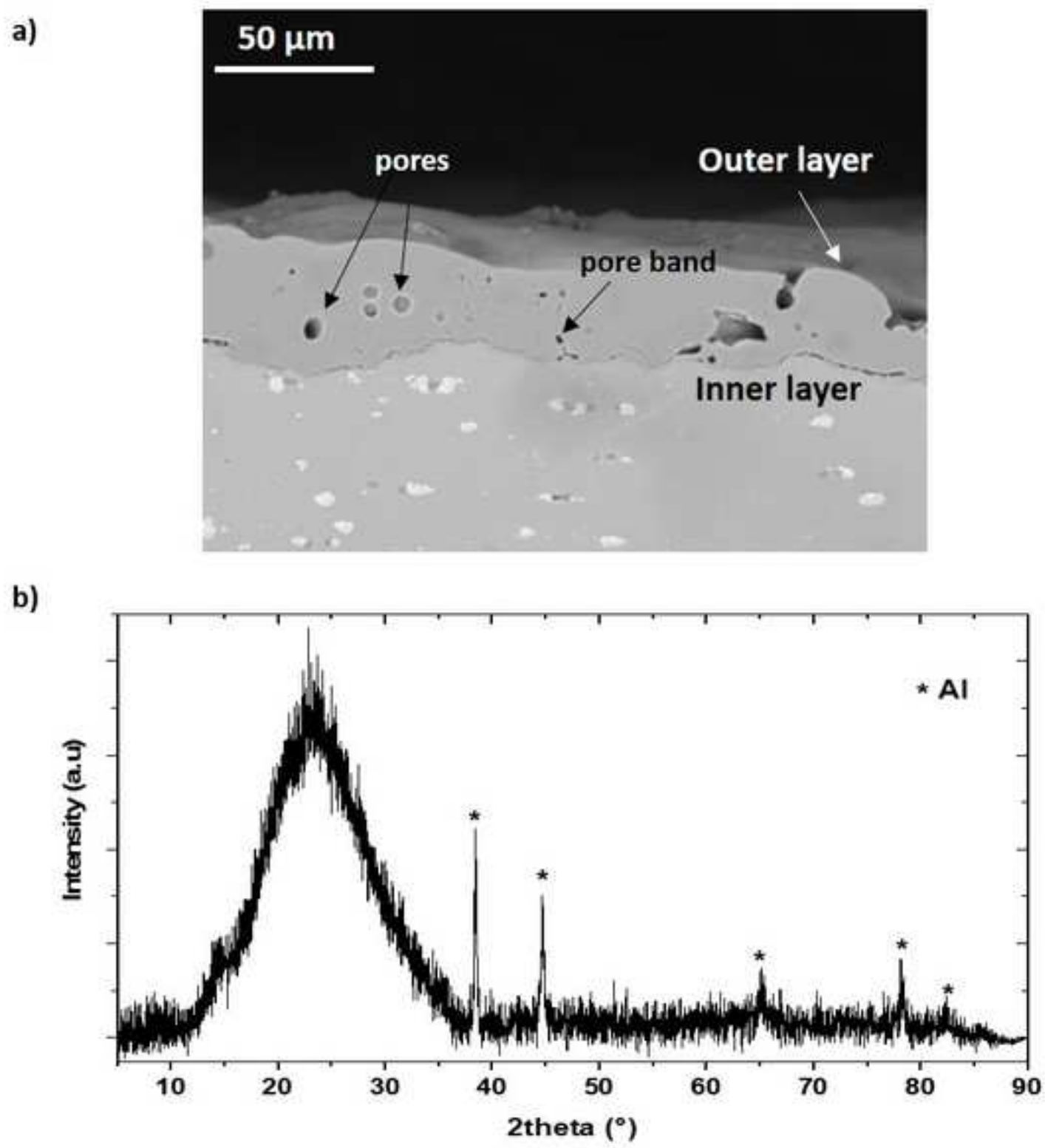

Figure 2

Click here to download high resolution image

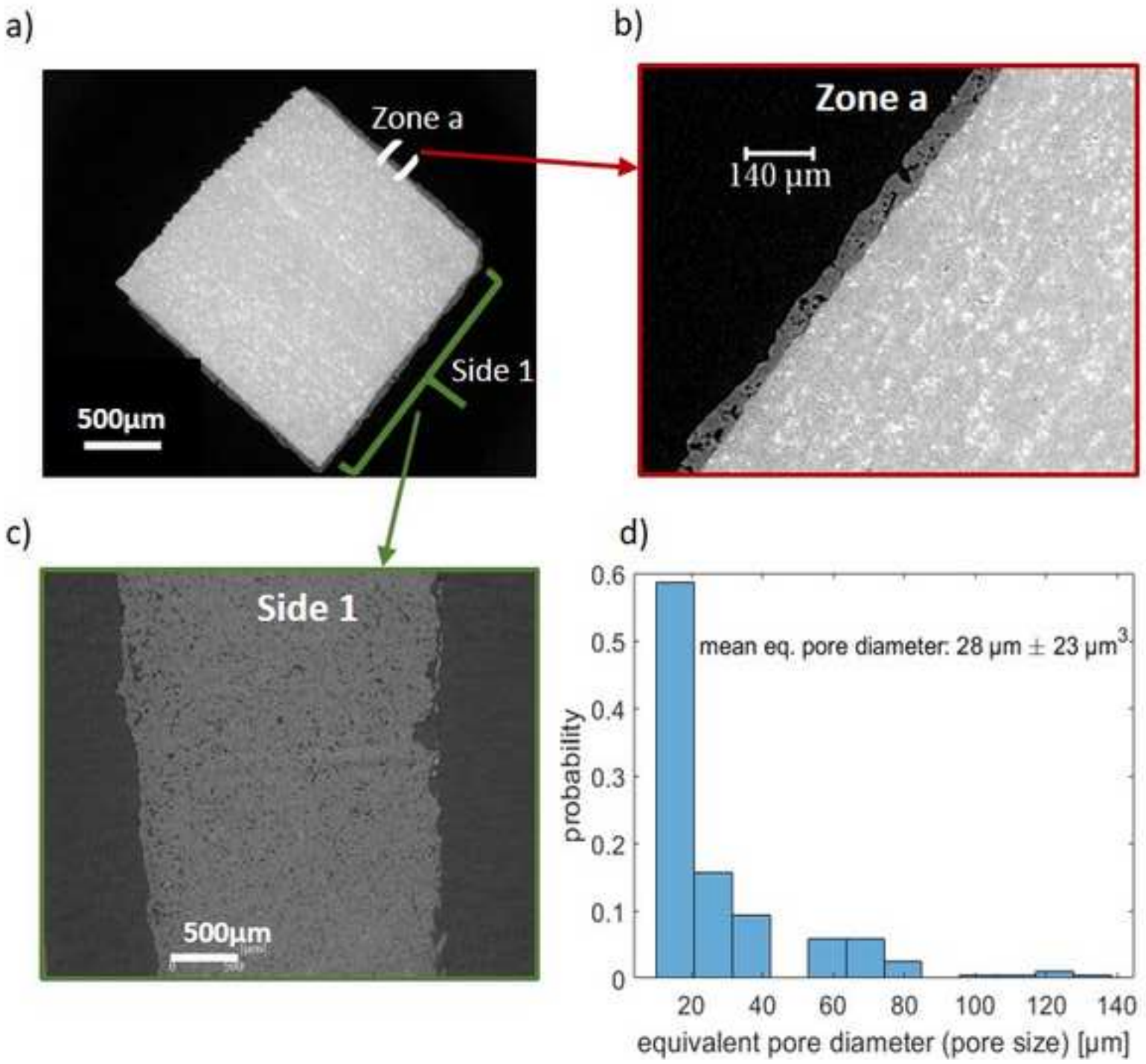

Figure 3
Click here to download high resolution image

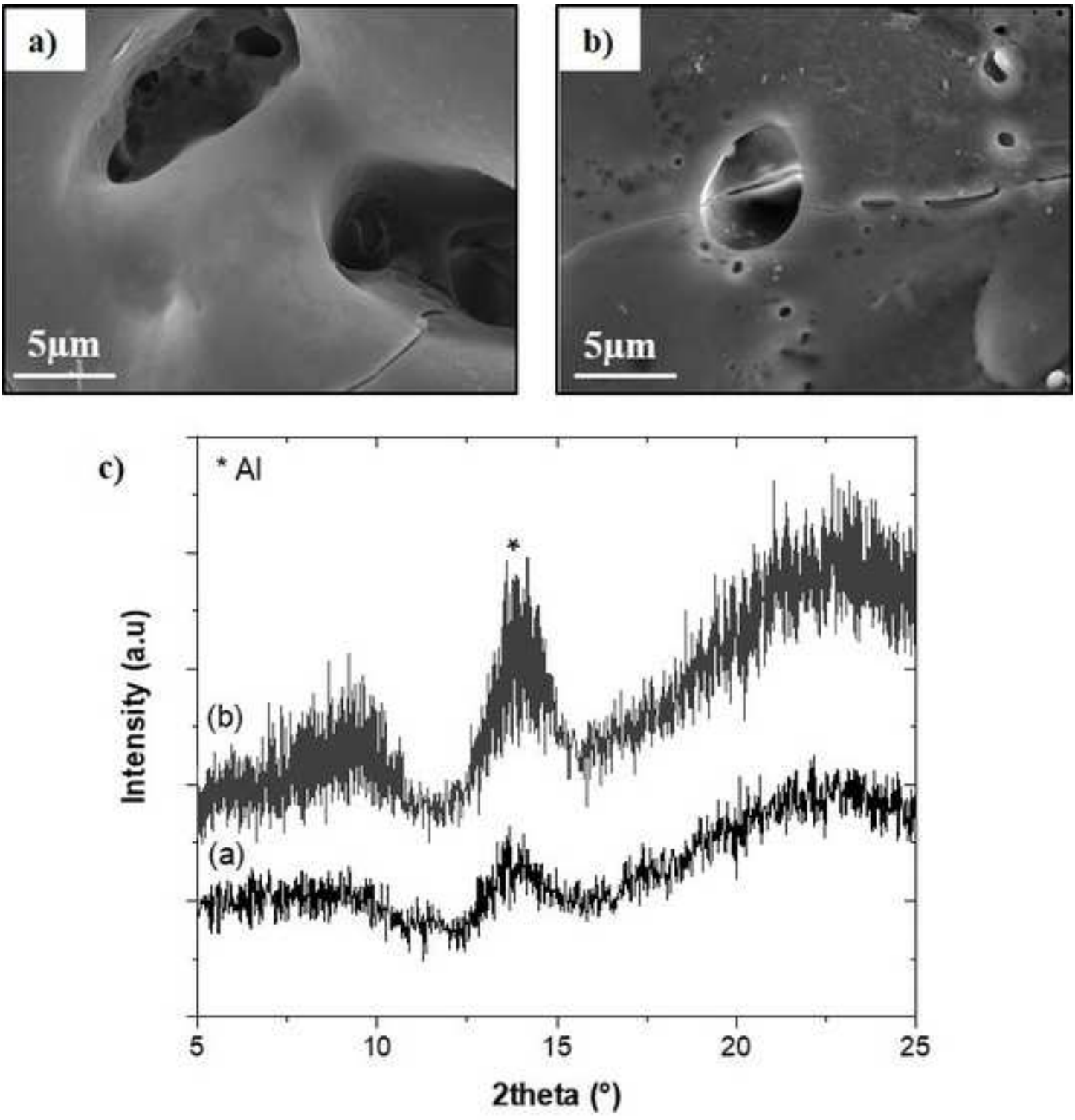

Figure 4

Click here to download high resolution image

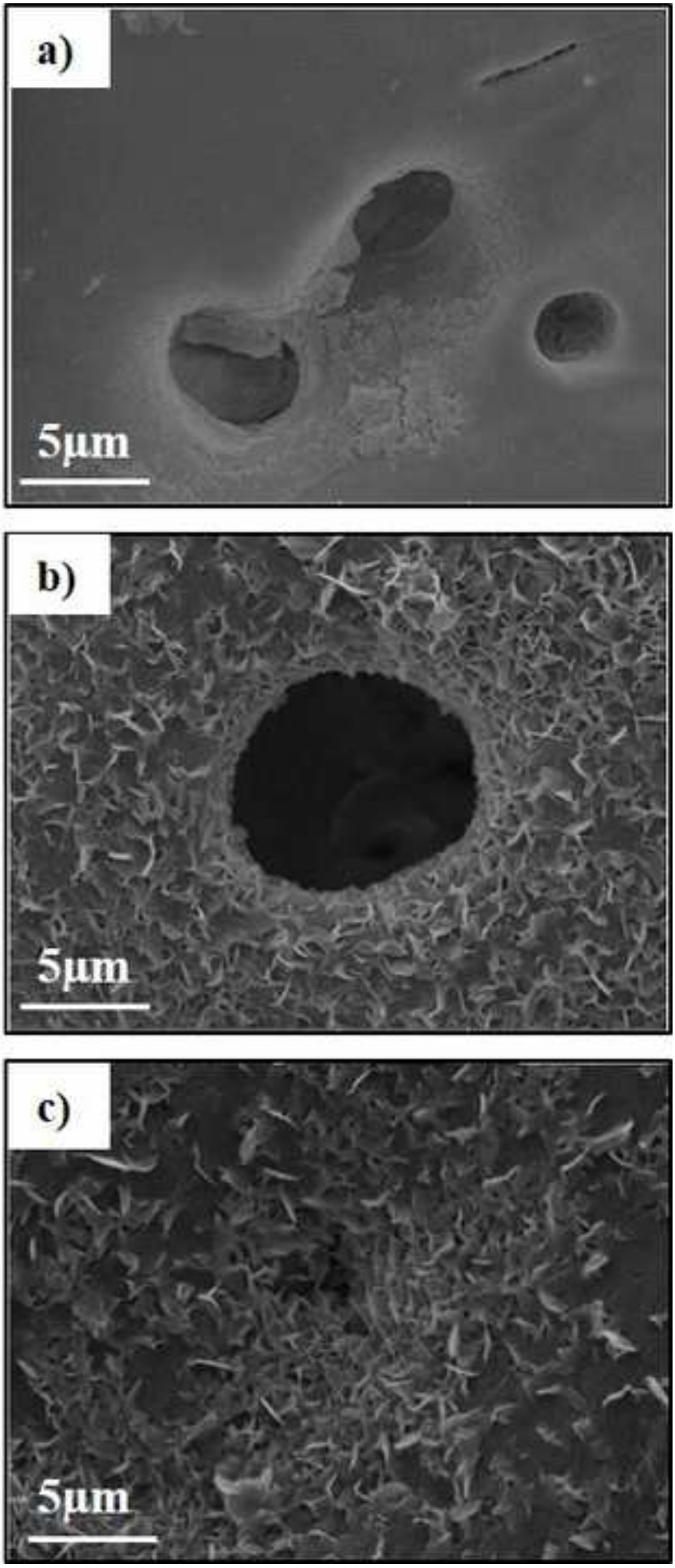

Figure 5

Click here to download high resolution image

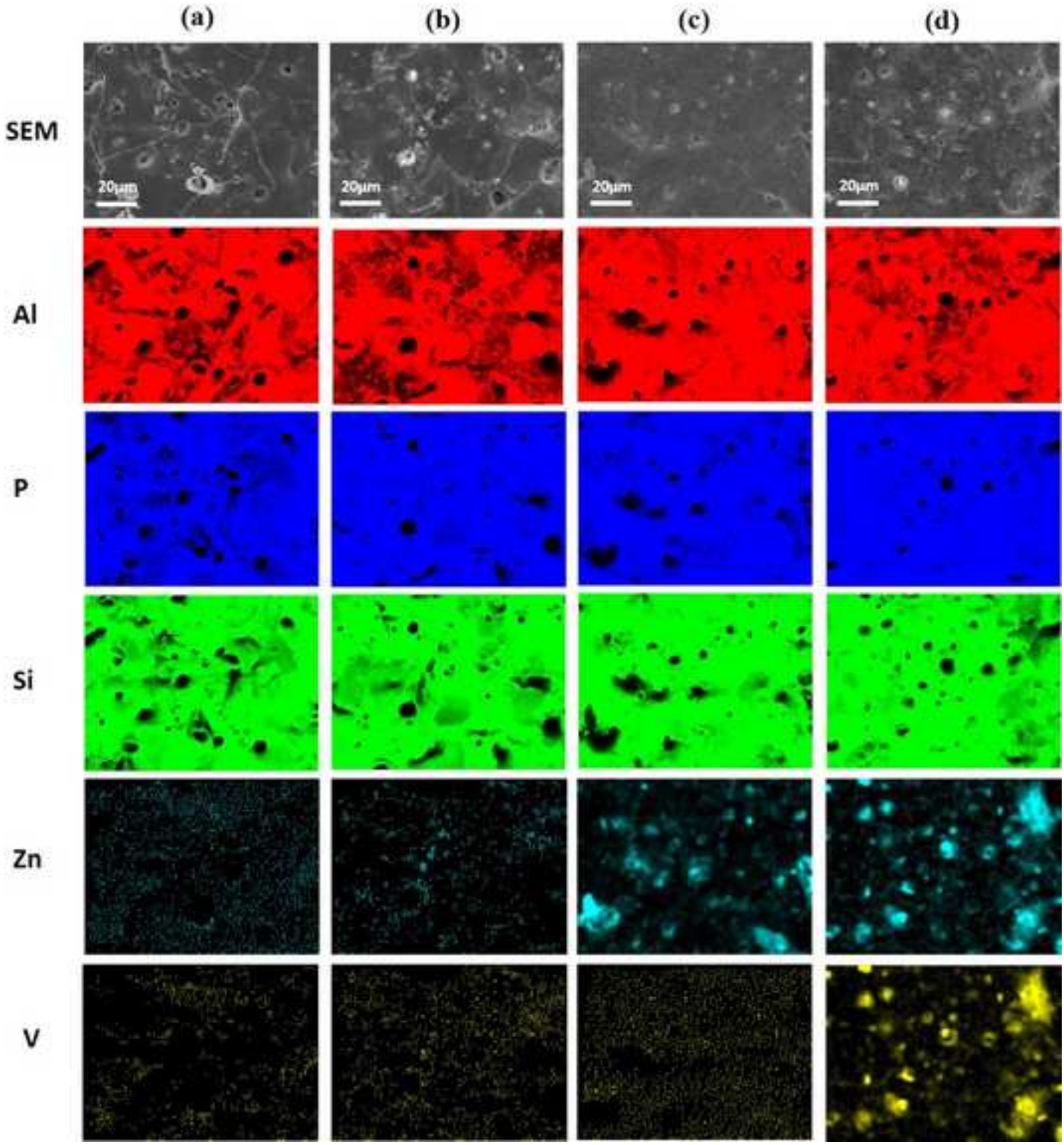

Figure 6

Click here to download high resolution image

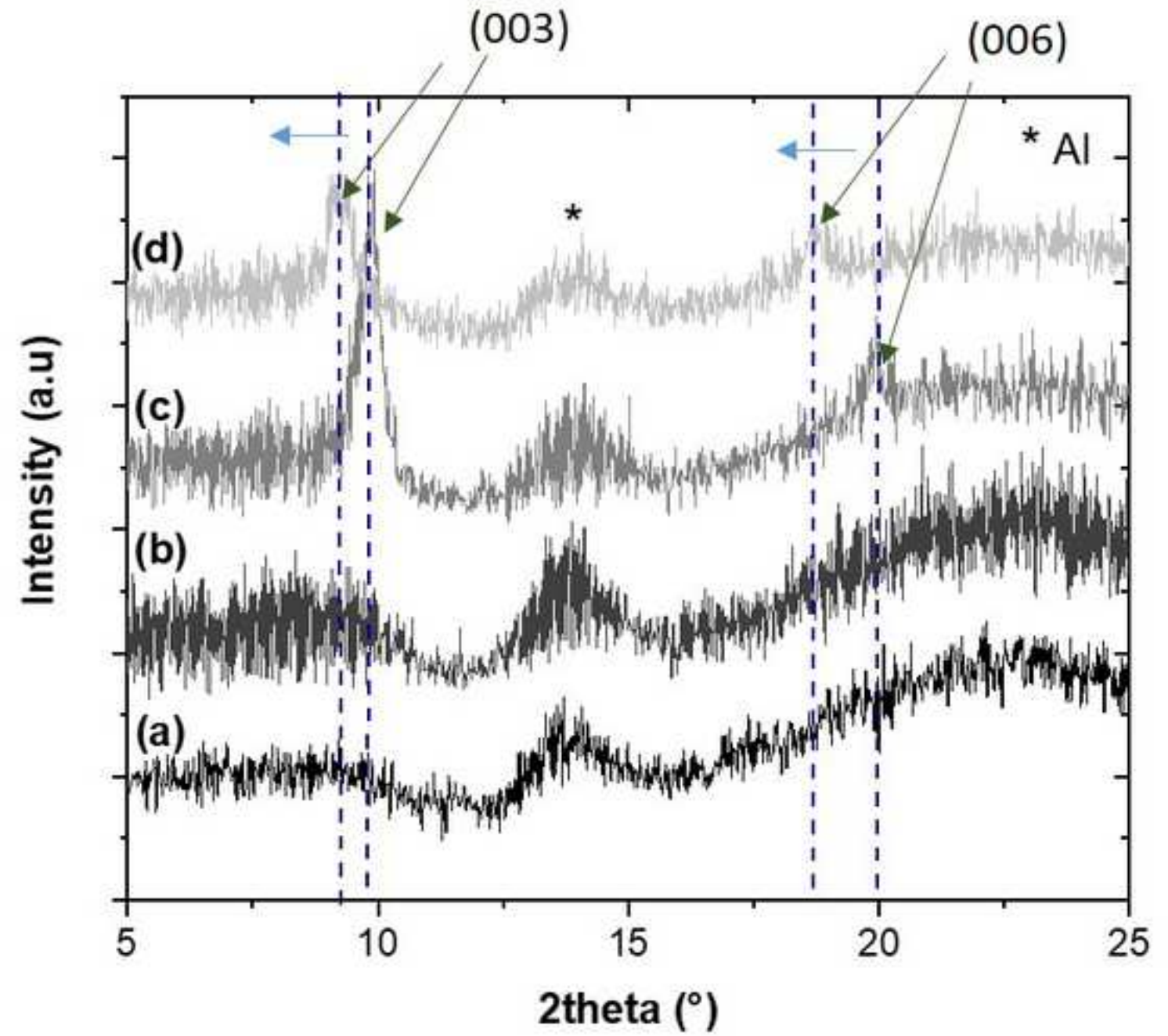

Figure 7

Click here to download high resolution image

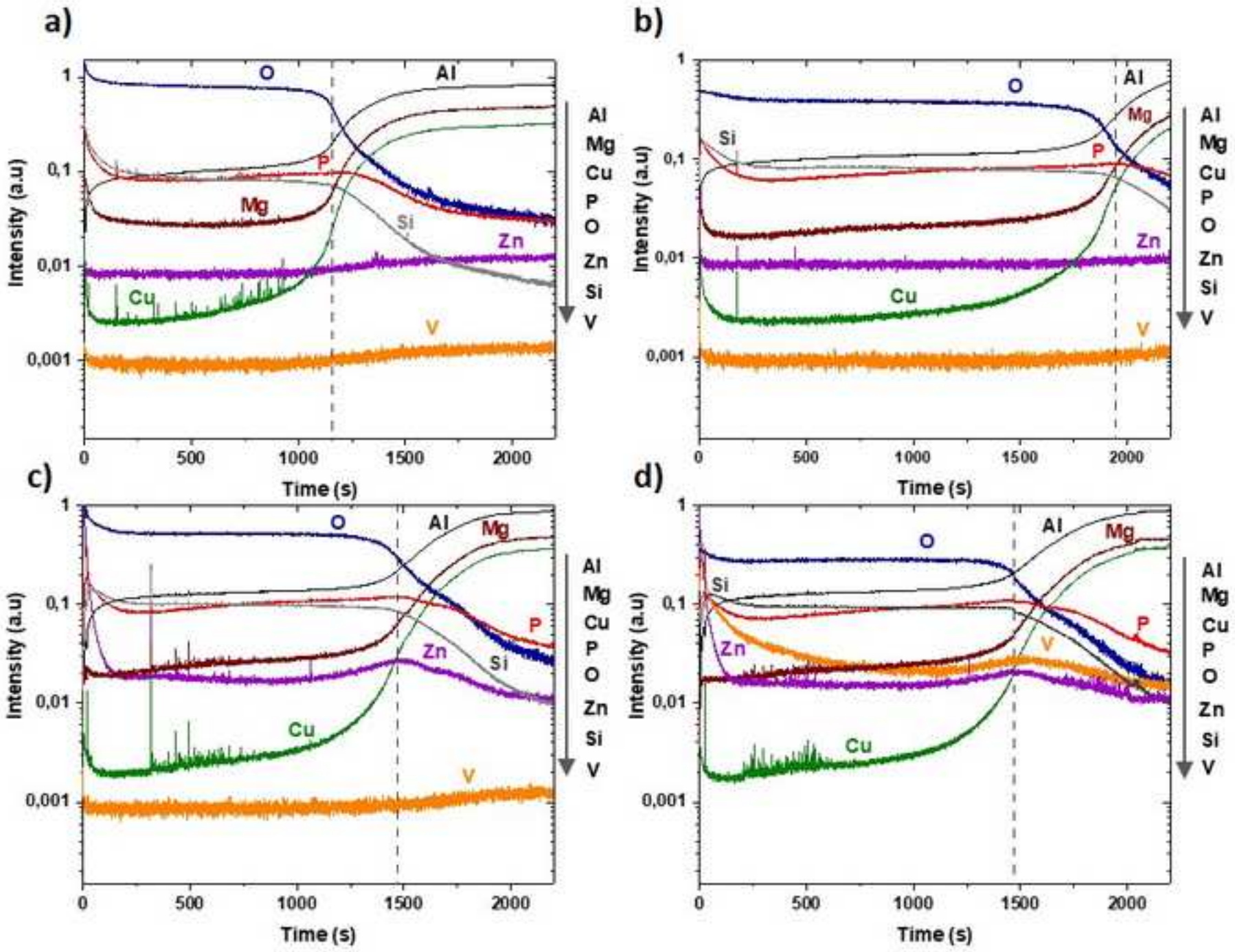

Figure 8
Click here to download high resolution image

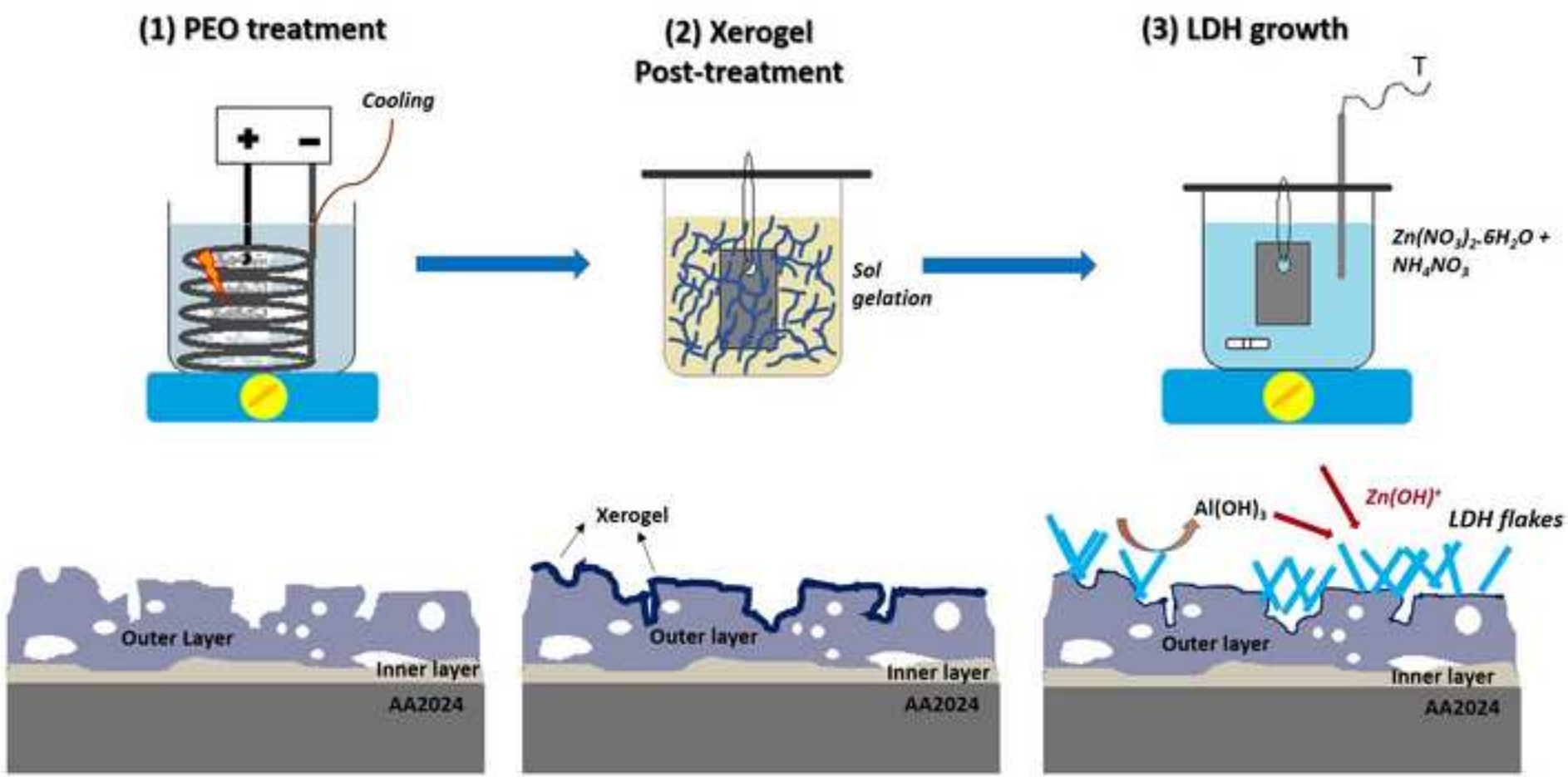

Figure 9

Click here to download high resolution image

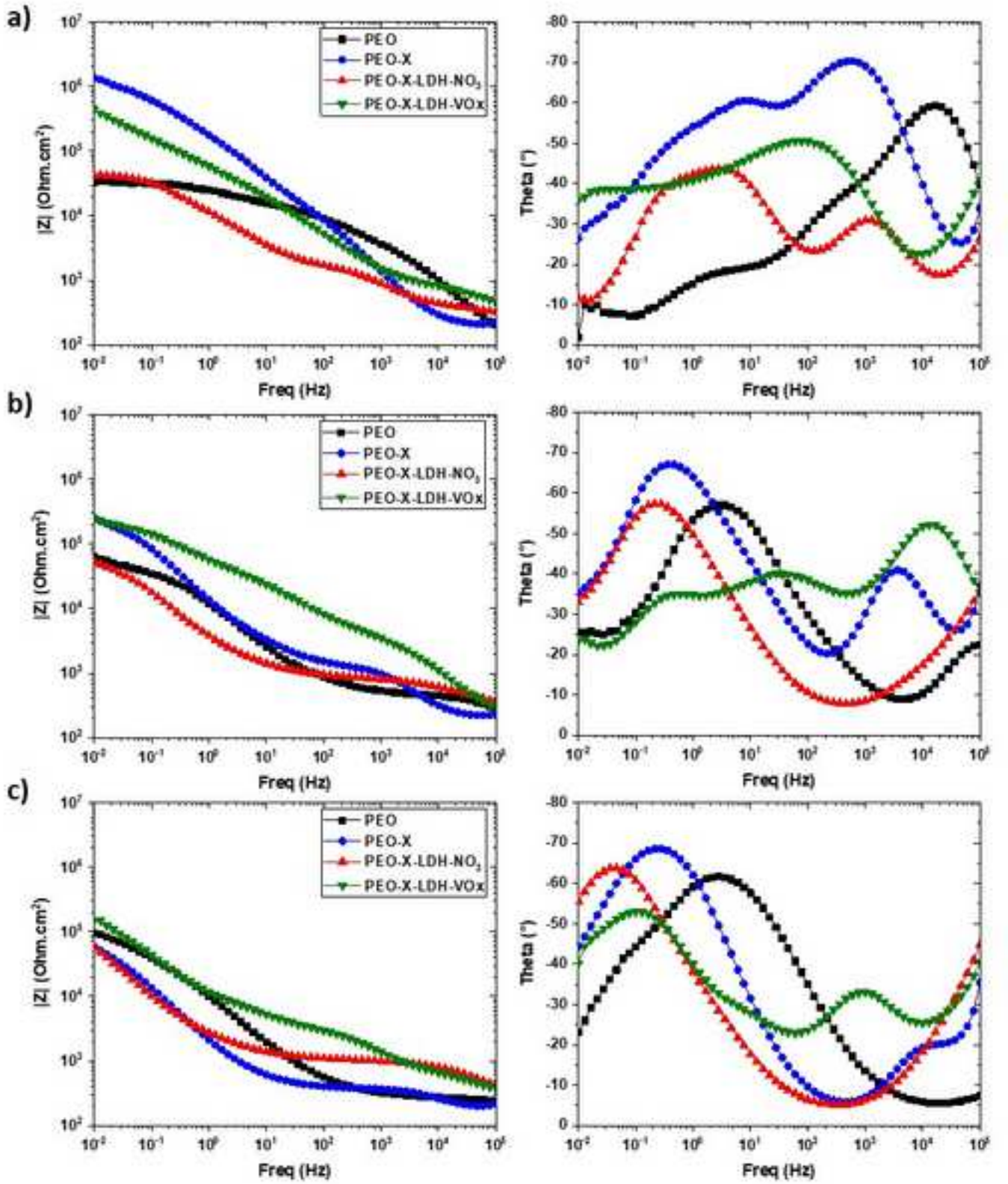

Figure 10

Click here to download high resolution image